Met. Mater. Int., Vol. 17, No. 3 (2011), pp. 383~388
doi: 10.1007/s12540-011-0003-9 Published 29 June 2011

High Temperature Deformation Behavior of Mg-Sn(-Zn) Alloy

Do H. Kim[1,*], H. K. Lim[1], Y. K. Kim[1], J. S. Kyeong[1], W. T. Kim[2], and D. H. Kim[1]

[1]Center for Noncrystalline Materials, Dept. of Metallurgical Eng. Yonsei University,
134 Shinchon-dong, Seodaemun-gu, Seoul 120-749, Korea
[2]IT Division, Cheongju University,
36 Naedeok-dong, Sangdang-gu, Cheongju-si, Chungbuk 360-764, Korea

(received date: 5 December 2009 / accepted date: 15 April 2011)

In the present study, we have investigated the high temperature deformation behavior of Mg-Sn(-Zn) based alloy systems in comparison with that of Mg-Al alloy. Compared with Mg-Al alloy, Mg-Sn alloy exhibits significantly refined grain structure and high ductility due to the presence of fine Mg_2Sn particles in the α-Mg matrix, for example, 184 % at 350 °C under a strain rate of 1×10^{-3} s^{-1}. When Zn is added to the Mg-Sn alloy, the elongation to failure remarkably increases from 184 % (Mg-Sn alloy) to 310 % under a strain rate of 1×10^{-3} s^{-1}. Such an improvement in ductility is due to the significantly refined grain structure that results from the addition of Zn.

Keywords: Mg-Sn alloy, high temperature deformation, ductility

1. INTRODUCTION

Mg alloys have shown great potential as structural materials for automotive and aerospace industries due to their low density and relatively high strength [1]. However, their inherent disadvantages, such as poor corrosion resistance, poor creep resistance and low formability have restricted their wide application as structural materials. To overcome these drawbacks, recently, a large amount of research is being performed on Mg-Sn based alloys. It has already been shown that the addition of Sn as a major alloying element in Mg alloys improves their corrosion resistance [2]. According to the Mg-Sn binary phase diagram [3], a larger amount of Sn is soluble in a-Mg, i.e. its solubility limit is about 14 wt.% at a eutectic temperature of 561 °C. Moreover, in the Mg-Sn binary system, there is only one inter-metallic compound, Mg_2Sn phase, exhibiting high thermal stability due to its high melting point of 770 °C. Besides this, compared to other solute elements used for commercial Mg alloys, such as Al, Zn, and Mn, Sn has the lowest diffusivity level in Mg [4]. All these points suggest that a high temperature strength Mg-Sn based alloy can be enhanced by utilizing precipitation hardening or second phase hardening. As a result, there have been many reports dealing with the excellent creep resistance of Mg-Sn based alloys [5-12]. However, there have been few reports on the high temperature formability and hot working behavior of Mg-Sn based alloys. Prasad et al. have reported on the extrusion of ternary Mg-3Sn-1Ca (wt.%) alloy with a fully recrystallized microstructure by introducing a processing map [13]. Sasaki et al. have reported that the quaternary Mg-2.2Sn-0.5Zn-1.0Al (at.%) alloy shows excellent extrudability at the relatively low temperature of 250 °C, and that it retains a high level of yield strength [14]. However, these previous reports have only focused on the hot working behavior starting from as-cast ingots. Moreover, there have been few reports on the high temperature deformation behavior of Mg-Sn based alloys.

It is well known that due to their limited slip systems, Mg alloys normally exhibit low formability at room temperature [15]. To obtain the adequate ductility required for plastic forming, Mg alloys need to be deformed above ~200 °C. It is generally known that there are two major mechanisms by which enough ductility for high temperature deformation can be provided, i.e., superplasticity and dislocation glide controlled creep [16]. Superplastic forming is possible when an ultra fine-grained microstructure is introduced, and when this microstructure should be accompanied by severe plastic deformation processing. However, the superplastic forming process has some disadvantages, such as high cost and small product size. Introduction of high ductility by the dislocation glide controlled creep mechanism has been observed in coarse-grained Mg-Al solid solution alloys [17]. Although high ductility can be obtained by the dislocation glide controlled creep mechanism, a very low strain rate is required during deformation [18].

*Corresponding author: dohkim@yonsei.ac.kr

Since there have been very few previous reports on the high temperature formability of Mg-Sn based alloys, the present study intends to investigate the detailed high temperature deformation behavior of Mg-1.5 at.% Sn and Mg-1.5 at.% Sn-0.8 at.% Zn alloy sheets fabricated by a hot-rolling process. Since most of the superplastically formable Mg alloys reported so far are based on the Mg-Al system, the experimental results for the binary Mg-Sn alloy have been compared with those for the binary Mg-1.5 at.% Al alloy.

2. EXPERIMENTAL PROCEDURE

Mg-1.5 at.% Sn, Mg-1.5 at.% Al and Mg-1.5 at.% Sn-(0.1 at.%, 0.4 at.%, 0.8 at.%) Zn alloys were prepared using high purity metals. These alloys were melted in an electrical resistance furnace under an $SF_6 + CO_2$ protective gas atmosphere. Molten metal was poured into a preheated (100 ℃) rectangular steel mold of 1.5 cm thickness, 6 cm width, and 10 cm height. Prior to the hot rolling, in order to eliminate solute segregation, homogenization treatment was conducted at 450 ℃ and 350 ℃ for Mg-Sn(-Zn) and Mg-Al alloys, respectively, for 24 h. After homogenization treatment, the samples were immediately quenched in cold water in order to prevent subsequent precipitation, which could bring about harmful effects during the hot working process.

To obtain a fine-grained microstructure, the cast ingots (70 mm × 50 mm × 10 mm) were hot-rolled to a final thickness of 1 mm (total reduction : 90 %). The ingots preheated at 350 ℃ for 15 min. were rolled with a maximum reduction ratio of 30 % per pass. The rolls were preheated to 100 ℃.

A uniaxial tensile test and strain-rate-change (SRC) test were conducted using dog-bone specimens with a gauge length of 10 mm. In order to obtain similar microstructures, different annealing conditions were applied prior to mechanical testing, i.e. 350 ℃ for 30 min. and 300 ℃ for 15 min. for Mg-Sn(-Zn) and Mg-Al alloys, respectively. The longitudinal direction of the tensile test specimens was parallel to the rolling direction. Uniaxial tensile tests were carried out at a temperature range from room temperature to 400 ℃ with a strain-rate range between 1×10^{-4} s^{-1} and 1×10^{-2} s^{-1}. SRC tests covering the strain-rate range from 5×10^{-6} s^{-1} to 1×10^{-1} s^{-1} were performed at a temperature range from 300 ℃ to 400 ℃. The tensile jig was heated inside the furnace, and then the specimen was inserted into the heated jig. The specimen was held for about 20 min. prior to the tensile test. To maintain the steady-state stress and keep grain growth rate to a minimum, a decremental step SRC test [19] was performed. SRC test results were used to determine strain rate sensitivities depending on temperature. Steady-state flow stress values for nine different strain-rate conditions were picked up and strain hardened and strain softened flow stress values were excluded.

The microstructure was observed with optical microscopy (OM; Leica DMRM), scanning electron microscopy (SEM; JEM 2001) and transmission electron microscopy (TEM; JEM 2000 EX). Specimens for TEM were prepared by an ion milling method (Gatan, model 600) under circulating LN_2 cooling conditions. The mean grain size (d) was measured by linear intercept method using the equation $d = 1.74L$, where L is the linear intercept grain size determined by optical microscopy.

3. RESULTS

Figure 1 shows optical micrographs obtained from static annealed Mg-1.5 at.% Sn, Mg-1.5 at.% Al and Mg-1.5 at.% Sn-0.8 at.% Zn alloy sheets after hot rolling. Different annealing conditions for Mg-Sn(-Zn) and Mg-Al alloys, i.e. 350 ℃ for 30 min. in Mg-Sn(-Zn) alloys and 300 ℃ for 15 min were applied to obtain a similar grain size in binary Mg-Sn and Mg-Al alloys, i.e. to investigate the high temperature deformation behavior starting from the similar grain size microstructure. The grain size in Mg-Sn and Mg-Sn alloys was similar, ~16.7 and ~19.3 mm, respectively, but was significantly smaller in the Mg-Sn-Zn alloy, i.e. ~9.35 mm.

Figure 2(a) describes the variations of elongation to failure in the three alloys obtained from the tensile test under an initial strain rate of 1×10^{-3} s^{-1}. Although the Mg-Sn and Mg-Al alloys exhibited a similar level of elongation to failure below 325 ℃, that value for the Mg-Sn alloy increased sig-

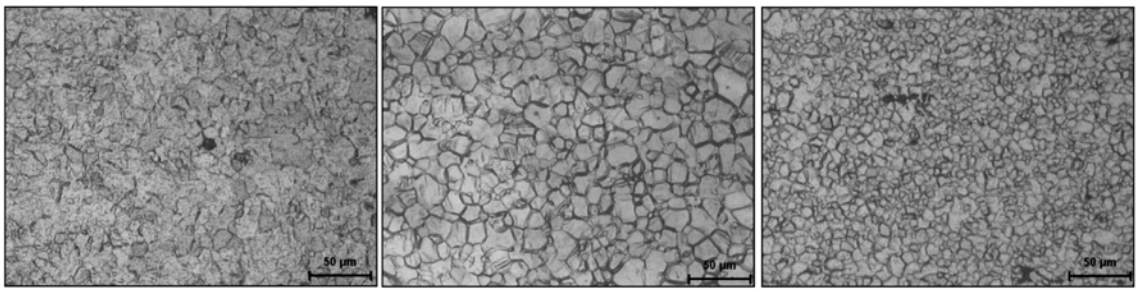

Fig. 1. Optical micrographs obtained from (a) Mg-Sn alloy annealed at 350 ℃ for 30 min., (b) Mg-Al alloy annealed at 300 ℃ for 15 min. and (c) Mg-Sn-Zn alloy annealed at 350 ℃ for 30 min, respectively.

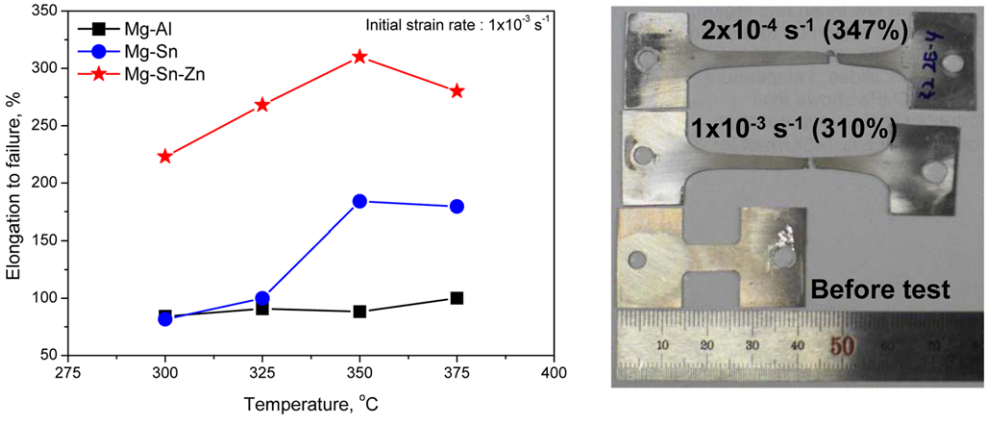

Fig. 2. (a) The variations of elongation to failure as a function of temperature in three different alloys and (b) surface appearances of Mg-Sn-Zn alloy tested up to failure at 350 °C.

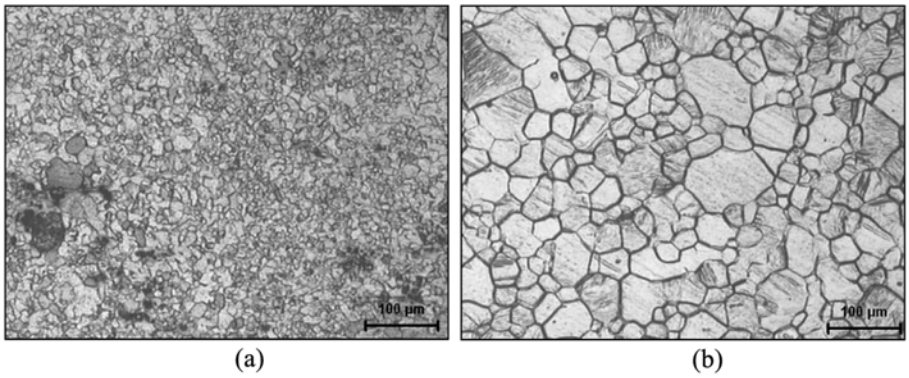

Fig. 3. Microstructures obtained from the specimen tested at 350 °C at a strain rate of 1 × 10^{-3} s^{-1} of (a) Mg-Sn and (b) Mg-Al alloy. (c) Bright field TEM micrograph of same Mg-Sn alloy.

nificantly above the test temperature of 350 °C. Also, at the test temperature of 350 °C, the Mg-Sn-Zn alloy showed the highest level of elongation to failure: compared with the Mg-Sn alloy, this elongation to failure was remarkably improved from 184 % to 310 % at 350 °C. With decreasing strain rate, the level of the elongation to failure was further improved, for example, it reached 347 % at a strain rate of 2 × 10^{-4} s^{-1}, as can be seen in Fig. 2(b).

Figure 3 provides optical micrographs obtained from both binary alloys tested at 350 °C with an initial strain rate of 1 × 10^{-3} s^{-1}. Before the tensile test, in order to obtain similar grain size in both alloys, different annealing conditions were applied, as described earlier. After the tensile test, similar grain size was retained in the Mg-Sn alloy, as shown in Fig. 3(a). However, significant grain growth occurred in the Mg-Al alloy after the tensile test at 350 °C (Fig. 3(b)).

Figure 4 shows the variations of flow stress as a function of strain rate obtained from a series of SRC tests at 350 °C. Strain rate sensitivity, *m*, is defined by the following equation;

$$m = \frac{(\partial \log \sigma)}{(\partial \log \dot{\varepsilon})}$$

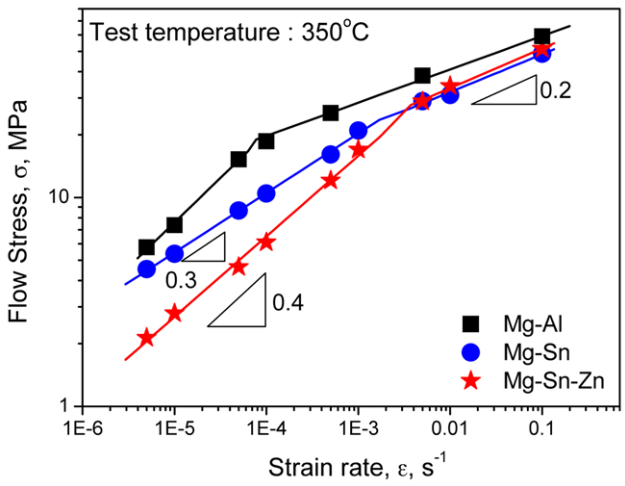

Fig. 4. The variations in flow stress as a function of strain rate in three different alloys at 350 °C.

where σ and $\dot{\varepsilon}$ represent flow stress and strain rate, respectively, which values can be obtained from the results shown in Fig. 4. The three alloys showed two distinct ranges exhib-

iting low and high strain rate sensitivity. In the case of the Mg-Sn alloy, the strain rate sensitivity, *m,* in the lower strain rate region up to 2×10^{-3} s^{-1} was estimated to be 0.3, while it was estimated to be 0.2 in the higher strain rate region above ~2×10^{-3} s^{-1}. Strain rate sensitivity of the Mg-Al alloy was higher than that of the Mg-Sn alloy, i.e. 0.4 up to a strain rate of 8×10^{-4} s^{-1}; it then decreased to ~ 0.2 with further increase of strain rate. In particular, the range of the strain rate exhibiting the higher strain rate sensitivity of ~0.4 in the Mg-Al alloy was much smaller (up to 8×10^{-4} s^{-1}) than that for the high strain rate sensitivity of ~ 0.3 in the Mg-Sn alloy (up to 2×10^{-3} s^{-1}). The high strain rate sensitivity regime (~ 0.4) in the Mg-Sn-Zn alloy was the largest among the three alloys (up to 5×10^{-3} s^{-1}). The strain rate sensitivity in the low strain rate regime increased from ~ 0.3 to ~ 0.4 as a result of the addition of Zn.

4. DISCUSSION

Recently, the Mg-Sn alloy system has been shown to exhibit high creep and corrosion resistance. In contrast this general awareness for the Mg-Sn alloy, the present study shows that Mg-Sn alloy rolled sheets exhibit high elongation to failure at 350 °C. A key factor that can be considered as a reason for such high ductility is the stable grain structure during deformation. To identify a possible reason for such a stable microstructure after the high temperature tensile test, the microstructure of annealed Mg-Sn alloy was examined by TEM (Fig. 5(a)). As can be seen in the bright-field TEM image, near- spherical-shaped particles, 100 nm to 600 nm in diameter, were distributed throughout the a-Mg matrix not only at the grain boundary but also inside the grains. The particles were identified as the Mg_2Sn phase, as can be seen in the inserted selected area diffraction pattern (SADP) taken from the particle marked with an arrow. The SADP was identified as the [012] zone of the face-centered cubic structure of the Mg_2Sn phase. It is clear that due to the grain boundary pinning effect by the Mg_2Sn particles the grain size remained almost constant even after long term exposure at high temperature.

Since the Mg-Sn system has high solubility of Sn at high temperature, it consists of a high volume fraction of Mg_2Sn precipitates (~4.72 %), as shown in Fig. 5(b). These precipitates play an important role in inhibiting grain growth during deformation. Maximum grain size to inhibit grain growth by the Mg_2Sn precipitates can be simply estimated by the Zener limiting grain size relationship between spherical particles and grain boundary, shown below [20];

$$\overline{D}_{\max} = \frac{4r}{3f}$$

where r is the particle radius and f is the volume fraction of particles. The average radius and volume fraction of Mg_2Sn precipitates were estimated to be ~ 250 nm and ~ 4.72 %, respectively, as can be seen in Fig. 5(b). Using these values, maximum grain size was calculated to be ~ 7.06 mm, indicating that the Mg_2Sn phase certainly plays a role in retaining the fine grain structure during hot deformation.

The experimental results indicate that the addition of Zn in the Mg-Sn alloy leads to not only grain refinement but also to a remarkable improvement of elongation to failure at elevated temperature. Such a favorable microstructure for high temperature deformation can also be percepted from the initial as-cast microstructure. Figure 6 shows optical micrographs obtained from as-cast Mg-1.5 at.% Sn-0.1 at.% Zn, Mg-1.5 at.% Sn-0.4 at.% Zn and Mg-1.5 at.% Sn-0.8 at.% Zn alloys, revealing that dendrite arm spacing (left side) and grain size (right side) become significantly finer with increasing Zn content in the Mg-Sn alloy. While 0.1 at.% Zn alloy shows relatively coarse grain size at a millimeter scale, 0.8 at.% Zn alloy consists of grains with a size of a few hundreds of micrometers. Since the same casting process was applied, nucleation rate can be considered to be similar. Therefore, the grain size refinement that results from the addition of Zn can be interpreted by considering the growth restricting factor (GRF) during solidification. During solidification of the

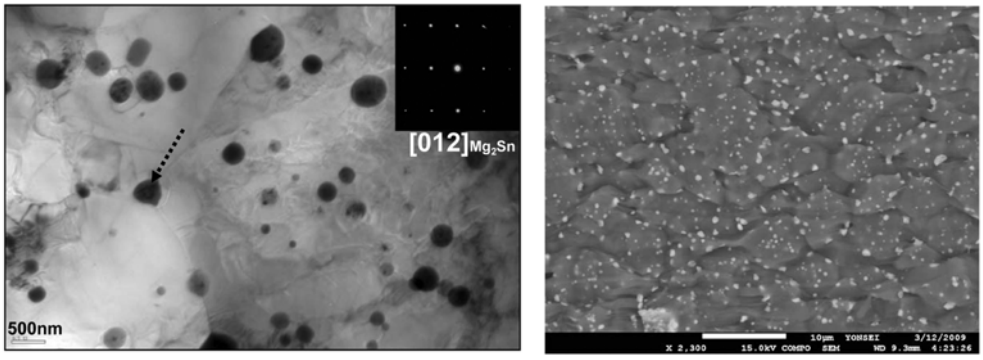

Fig. 5. (a) Bright field TEM micrograph of Mg-Sn alloy tested at 350 °C at a strain rate of 1×10^{-3} s^{-1}. (b) Backscattered scanning electron micrographs of same alloy.

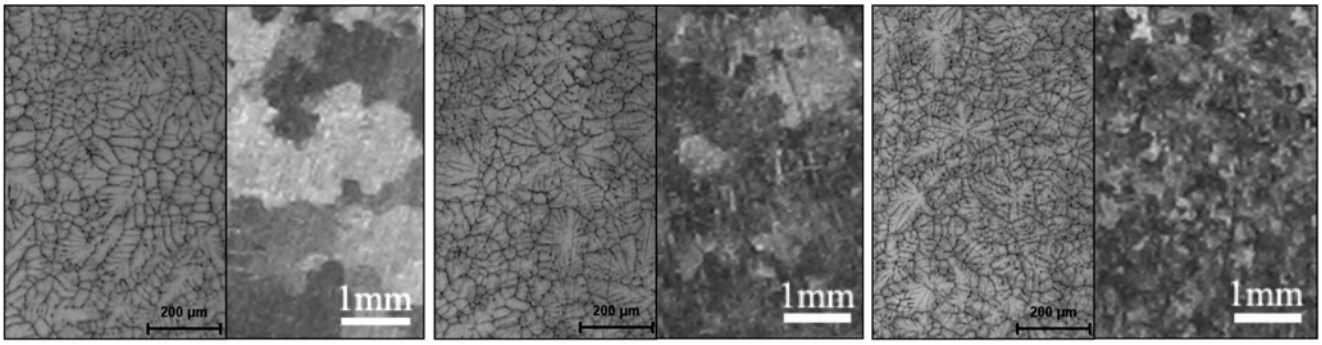

Fig. 6. Optical micrographs which show the effect of Zn on ac-cast microstructure of (a) Mg-1.5Sn-0.1Zn (at.%), (b) Mg-Sn-0.4Zn (at.%) and (c) Mg-1.5Sn-0.8Zn (at.%), respectively.

Table 1. Grain restriction factor of Mg-Sn, Mg-Zn and Mg-Sn-Zn alloys obtained from their thermodynamic data based on the respective phase diagrams

Alloys (at.%)	k_i	m	C_0	$m_iC_0(k_i-1)$
Mg-1.5Sn	0.29	-6.21	1.5	6.61
Mg-0.8Zn	0.1	-7.88	0.8	5.67
Mg-1.5Sn-0.8Zn				12.29

alloys, the solute composition gradient ahead of the interface introduces an additional change in the free energy, which corresponds to compositional undercooling. The criterion for compositional undercooling can be understood according to the following equation:

$$\frac{G_L}{R} \geq \frac{\sum m_i C_0 (k_i - 1)}{kD_L}$$

From this equation, it can be deduced that the growth rate of dendrites is inversely proportional to $\sum m_i C_0 (k_i - 1)$, where m is the liquidus slope, C_0 the bulk alloy composition in liquid and k_i the partition coefficient between solid and liquid. This term can be a measure of the growth restricting factor (GRF) by solute elements on the growth of the solid-liquid interface [21-23]. Table 1 reveals the calculated GRF values for Mg-Sn, Mg-Zn and Mg-Sn-Zn alloys using thermodynamic data based on the respective phase diagrams. It can be seen that the addition of Zn in the Mg-Sn alloy leads to a rise in the GRF value from 6.61 to 12.29, implying that Zn is a very effective dendrite refiner that can restrict dendrite growth during solidification. Therefore, the addition of Zn in the Mg-Sn system leads to an initial fine microstructure, resulting in significantly improved high temperature formability.

5. CONCLUSIONS

In the present study, we have investigated the high temperature deformation behavior of Mg-Sn(-Zn) based alloy systems in comparison with those using Mg-Al alloy. The Mg-Sn alloy shows high ductility: for example, 184 % at 350 °C under a strain rate of 1×10^{-3} s^{-1}. It is interesting that the Mg-Sn alloy shows high formability, even though we know that it has a high temperature creep resistance. The key factor that can be considered as responsible for this high ductility is stable grain structure during deformation. From the TEM analysis, it is clear that due to the grain boundary pinning effect by the Mg_2Sn particles the grain size remains almost constant even after long term exposure at high temperature. When Zn is added in the Mg-Sn alloy, the elongation to failure remarkably increases from 184 % (binary Mg-Sn alloy) to 310 %, under a strain rate of 1×10^{-3} s^{-1}. Such an improvement in ductility is due to the significantly refined grain structure that results from the addition of Zn. The addition of Zn leads to a fine dendrite structure in the Mg-Sn alloy during solidification. Thus, Zn is a very effective dendrite refiner that can restrict dendrite growth in the Mg-Sn alloy system. Therefore, the addition of Zn in the Mg-Sn system leads to an initial fine microstructure, resulting in significantly improved high temperature formability.

ACKNOWLEDGMENTS

This study was supported by a grant from the Fundamental R&D Program for Core Technology of Materials funded by the Ministry of Commerce, Industry and Energy, Republic of Korea, and the Global Research Laboratory Program of Korea Ministry of Science and Technology. One of the authors (W.T. Kim) thanks for a financial support from the Center for Advanced Materials Processing (CAMP) of the 21st Century Frontier R&D Program funded by the Ministry of Knowledge Economy (MKE), Republic of Korea.

REFERENCES

1. B. L. Mordike and T. Ebert, *Mater. Sci. Eng. A* **302**, 37 (2001).
2. T. A. Leil, K. P. Rao, N. Hort, C. Blawert, and K. U. Kainer, *Corrosion Behavior and Microstructure of a Broad Range*

of Mg-Sn-X Alloys, Magnesium Technology 2006, p. 281, TMS, Warrendale, PA, USA (2006).
3. C. R. Brooks, Heat Treatment, Structure and Properties of Nonferrous Alloys, p. 261, American Society for Metals, Metals park, OH, USA (1982).
4. J. Combronde and G. Brebec, *Acta met.* **20**, 37 (1972).
5. D. H. Kim, J. Y. Lee, H. K. Lim, J. S. Kyeong, W. T. Kim, and D. H. Kim, *Mater. Trans.* **49**, 2405 (2008).
6. D. H. Kang, S. S. Park, and N. J. Kim, *Mater. Sci. Eng. A* **413-414**, 555 (2005).
7. D. H. Kang, S. S. Park, Y. S. Oh, and N. J. Kim, *Mater. Sci. Eng. A* **449-451**, 318 (2007).
8. H. Liu, Y. Chen, Y. Tang, S. Wei, and G. Niu, *J. Alloy. Compd.* **440**, 122 (2007).
9. N. Hort, Y. Huang, T. A. Leil, P. Maier, and K. U. Kainer, *Adv. Eng. Mater.* **8**, 359 (2006).
10. T. A. Leil, Y. Huang, H. Dieringa, N. Hort, K. U. Kainer, J. Bursik, Y. Jiraskova, and K. P. Rao, *Mater. Sci. Forum.* **546-549**, 69 (2007).
11. A. L. Bowles, H. Dieringa, C. Blawert, N. Hort, and K. U. Kainer, *Mater. Sci. Forum.* **488-489**, 135 (2005).
12. S. Harosh, L. Miller, G. Levi, and M. Bamberger, *J. Mater. Sci.* **42**, 9983 (2007).
13. Y. V. R. K. Prasad, K. P. Rao, N. Hort, and K. U. Kainer, *Mater. Sci. Eng. A* **502**, 25 (2008).
14. T. T. Sasaki, K. Yamamoto, T. Honma, S. Kamado, and K. Hono, *Scripta mater.* **59**, 1111 (2008).
15. T. H. Courtney, *Mechanical behavior of Materials, 2nd ed.*, p. 160, 309, McGraw-Hill Co., Singapore (2000).
16. H. Somekawa, K. Hirai, H. Watanabe, Y. Takigawa, and K. Higashi, *Mater. Sci. Eng. A* **407**, 53 (2005).
17. S. W. Chung, H. Watanabe, W. J. Kim, and K. Higashi, *Mater. Trans.* **45**, 1266 (2004).
18. H. Watanabe, H. Tsutsui, Y. Mukai, M. Kohzu, S. Tanabe, and K. Higashi, *Int. J. Plast.* **17**, 387 (2001).
19. D. H. Bae and A. K. Ghosh, *Acta mater.* **48**, 1207 (2000).
20. D. A. Porter and K. E. Eastering, *Phase Transformation in Materials, 2nd ed.*, p. 291, Chapman & Hall London, UK (1992).
21. K. T. Kashyap and T. Chandrasherkar, *Bull. Mater. Sci.* **24**, 345 (2001).
22. H. K. Kim, D. H. Kim, J. Y. Lee, J. S. Kyeong, W. T. Kim, and D. H. Kim, *Met. Mater. Int*. **15**, 337 (2009).
23. B. J. Jung, M. J. Lee, and Y. B. Park, *Kor. J. Met. Mater.* **48**, 305 (2010).